

Reentrant Non-Hermitian Skin Effect Induced by Correlated Disorder

Wei-Wu Jin,^{1,*} Jin Liu,^{1,*} Xin Wang,² Yu-Ran Zhang,¹ Xueqin Huang,¹ Xiaomin Wei,¹ Wenbo Ju,^{1,†} Tao Liu,^{1,‡} Zhongmin Yang,^{1,3,4,§} and Franco Nori^{5,6,7}

¹*School of Physics and Optoelectronics, South China University of Technology, Guangzhou 510640, China*

²*Institute of Theoretical Physics, School of Physics, Xi'an Jiaotong University, Xi'an 710049, China*

³*Research Institute of Future Technology, South China Normal University, Guangzhou 510006, China*

⁴*State Key Laboratory of Luminescent Materials and Devices and Institute of Optical Communication Materials, South China University of Technology, Guangzhou 510640, China*

⁵*Theoretical Quantum Physics Laboratory, Cluster for Pioneering Research, RIKEN, Wako-shi, Saitama 351-0198, Japan*

⁶*RIKEN Center for Quantum Computing, Wako-shi, Saitama 351-0198, Japan*

⁷*Department of Physics, University of Michigan, Ann Arbor, Michigan 48109-1040, USA*

(Dated: October 16, 2024)

The interplay of non-Hermiticity and disorder drastically influences the system's localization properties, giving rise to intriguing quantum phenomena. Although the intrinsic non-Hermitian skin effect (NHSE) is robust against weak disorder even in a one-dimensional system, it becomes Anderson localization under strong disorder. Here, we study an Anderson localization-delocalization transition by coupling a strongly disordered Hatano-Nelson (HN) chain to a disordered Hermitian chain with their disorders anti-symmetrically correlated with each other. Regardless of the disorder strength, as the inter-chain coupling strength increases, an Anderson delocalization can occur. This leads to a reentrant NHSE due to the interplay of nonreciprocal hopping and correlated disorder. Furthermore, the Anderson localization-delocalization transition is well captured by the real-space winding number. This reentrant NHSE, under anti-symmetric disorder, is a remarkably nontrivial physical phenomenon without a Hermitian counterpart. We then experimentally test this phenomenology by implementing our model in electrical circuits, and observe the reentrant NHSE by measuring the voltage response.

The past few years have witnessed an explosion of interest in exploring exotic physics in non-Hermitian systems [1–19]. These systems include, but not limited to, classical optical platforms [20–28], electrical circuits [29–33], and open quantum systems with post-selection measurements [34, 35]. One of the striking physical phenomena in non-Hermitian systems is the non-Hermitian skin effect (NHSE) [3–6], where its bulk modes exhibit extensive sensitivity to imposed boundary conditions. A majority of these bulk modes under periodic boundary conditions (PBCs) collapse into localized edge modes under open boundary conditions (OBCs), forming skin modes. These skin modes originate from the intrinsic point-gap topology [6, 7]. Many exciting non-Hermitian phenomena without their Hermitian counterparts are related to NHSEs, e.g., breakdown of conventional Bloch band theory [3] and disorder-free entanglement phase transitions [18].

Disorder plays a vital role in determining the behavior of non-Hermitian systems in various aspects, including transport, entanglement and topology [36–50], and give rise to a plethora of exotic phenomena, e.g., the nonunitary scaling rule of the non-Hermitian localization [46], disorder-induced non-Bloch topological phase transitions [49] and coexistence of dynamical delocalization and spectral localization [48]. Hatano and Nelson first investigated the non-Hermitian extension of the one-dimension (1D) Anderson model with nonreciprocal hopping [36], revealing the unexpected

delocalization and appearance of skin modes for weak random potentials, while a 1D disordered Hermitian system is always localized [51]. This indicates that the non-Hermiticity can destroy Anderson localization in the 1D Hatano-Nelson (HN) chain [39]. By further increasing disorder strength, all the skin states becomes localized once more. However, it remains unclear whether a localization to delocalization transition with a reentrant NHSE can be realized in a strong disordered non-Hermitian system. As far as we know, the delocalization can occur via coupling the disordered chains in the Hermitian systems [52–58], which stimulates us to explore disordered non-Hermitian chains in a coupled ladder.

In this work, we theoretically study and experimentally observe the Anderson localization to delocalization transition by coupling the disordered HN chain to a disordered Hermitian chain with their disorders correlated with each other. Although each chain of the ladder is strongly disordered, a delocalization transition occurs, accompanied by the reentrant NHSE, if the random onsite potential in the HN chain is anti-symmetrically correlated to the one in the Hermitian chain. When the disorder strength becomes ultra-large to cause Anderson localization, the NHSE can resume by further increasing the coupling strength between the HN and Hermitian chains. The underlying mechanism is intuitively analyzed, and the localization-delocalization phase transition is characterized by the

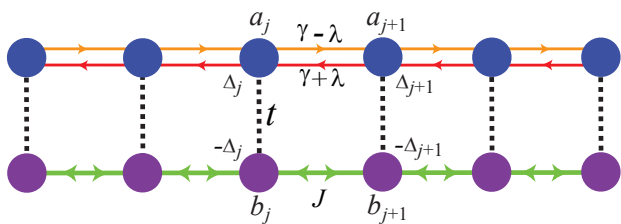


FIG. 1. **Coupled HN-Hermitian chains subject to correlated disorders.** Schematic showing a disordered HN chain (top) coupled to a disordered Hermitian chain (bottom). $\gamma \pm \lambda$ denote the asymmetric hopping strengths of the HN chain, J is the symmetric hopping strength of the Hermitian chain, and t is the symmetric hopping strength between two chains. When the HN chain is subjected to a strong random onsite potential Δ_j , the non-Hermitian skin-modes become Anderson-localized. While, the NHSE can be recovered if an anti-symmetric disorder is applied to the coupled Hermitian chain with its random onsite potential $-\Delta_j$.

real-space winding number. We implement our model in an electrical circuit platform, where the nonreciprocal hopping can be easily realized [31, 59]. The key features of our model are experimentally probed, which verifies our theoretical predictions.

Results

Theory

We start by considering a 1D non-Hermitian Hatano-Nelson (HN) chain with asymmetric hopping [36], which shows a NHSE. When the HN chain is subjected to the random onsite potential, the interplay of non-reciprocal hopping and disorder can result in delocalization with partially extended single-particle eigenstates for weak disorder strength [36–39, 46]. While further increasing disorder strength leads to Anderson localization in the HN chain. In this work, we show that the NHSE can be recovered, even in the ultra-strong disorder regime, by coupling the disordered HN chain to a disordered Hermitian chain with their disorders correlated with each other, as shown in Fig. 1.

The Hamiltonian of the hybrid system is written as

$$\begin{aligned} \hat{\mathcal{H}} = & \sum_j \left[(\gamma + \lambda) \hat{a}_j^\dagger \hat{a}_{j+1} + (\gamma - \lambda) \hat{a}_{j+1}^\dagger \hat{a}_j \right] \\ & + \sum_j \left(J \hat{b}_{j+1}^\dagger \hat{b}_j + t \hat{a}_j^\dagger \hat{b}_j + \text{H.c.} \right) \\ & + \sum_j \left(\Delta_j^{(a)} \hat{a}_j^\dagger \hat{a}_j + \Delta_j^{(b)} \hat{b}_j^\dagger \hat{b}_j \right), \end{aligned} \quad (1)$$

where \hat{a}_j^\dagger and \hat{b}_j^\dagger are creation operators for the HN chain and the Hermitian chain at j th unit cell, respectively; the asymmetric hopping is denoted by $\gamma \pm \lambda$; J is the symmetric hopping strength for the Hermitian chain; t is the coupling strength of two chains; and $\Delta_j^{(\mu)}$ ($\mu = a, b$) is the random onsite potential, applied to the HN

chain ($\mu = a$) and the Hermitian chain ($\mu = b$), which is uniformly sampled in $[-W/2, W/2]$, with W being the disorder strength.

Although the strong disorder leads to the localization of all the states in the HN chain, we will show that a reentrant NHSE can occur if an appropriately correlated disorder is applied to the coupled Hermitian chain. We consider two types of correlated disorder schemes: symmetric disorder with $\Delta_j^{(a)} = \Delta_j^{(b)} = \Delta_j$, and anti-symmetric disorder with $\Delta_j^{(a)} = -\Delta_j^{(b)} = \Delta_j$.

Figure 2 plots the probability density distributions of eigenstates under strong onsite disorder, and the corresponding complex eigenenergies under PBC (blue dots) and OBC (red dots). All the states in the coupled HN-Hermitian chains remain localized in the presence of both uncorrelated disorder [see Fig. 2a] and symmetrically correlated disorder [see Fig. 2b]. The breakdown of NHSE is also indicated by the absence of point gaps in Fig. 2d and 2e, respectively. However, when anti-symmetrically correlated disorder is introduced, the complex eigenspectrum (blue dots) for PBC forms two point gaps for a large inter-chain coupling strength t [see Fig. 2f], encircling the eigenenergies (red dots) for OBC. All the states inside the point gap are localized at the left boundary, as shown in Fig. 2c, where a reentrant NHSE occurs. Note that the eigenstates in the coupled two-Hermitian chains remain localized in spite of anti-symmetric disorder, as discussed below. This indicates that the reentrant NHSE of a disordered nonreciprocal chain, coupled to a Hermitian chain subject to the anti-symmetrical disorder, is a remarkably nontrivial physical phenomenon without a Hermitian counterpart.

The hidden physical mechanism can be intuitively understood in the concrete case of the strong inter-chain coupling with $|t| \gg |J|, |\gamma \pm \lambda|, |\Delta_j|$ for both symmetric and anti-symmetric disorder configurations (see details in the Methods section). In this strong inter-chain coupling limit, after rewriting $\hat{\mathcal{H}}$ in the new basis $|\alpha_{\pm}, j\rangle = \hat{\alpha}_{\pm, j}^\dagger |0\rangle$, with $\hat{\alpha}_{\pm, j} = (\pm \hat{a}_j + \hat{b}_j)/\sqrt{2}$, we obtain an effective nonreciprocal Creutz ladder subject to the onsite random potential $\Delta_j \pm t$ and $\pm \sqrt{t^2 + \Delta_j^2}$ for the symmetric and anti-symmetric disorder configurations, respectively. For the symmetric disorder scheme, this nonreciprocal Creutz ladder becomes Anderson localization for strong disorder Δ_j . However, for the anti-symmetric disorder case, the effective disorder strength \tilde{W} of the Creutz ladder becomes $\tilde{W} < W^2/|8t|$. In the strong coupling limit, with $|t| \gg W$, the disorder strength \tilde{W} of the nonreciprocal Creutz ladder is much smaller than the asymmetric hopping strength λ . Although an arbitrarily small amount of disorder leads to Anderson localization in 1D Hermitian systems [51], it has been shown that the interplay of nonreciprocal hopping and disorder causes Anderson transition [36, 39]. Therefore, the increasing inter-chain hopping t eventually

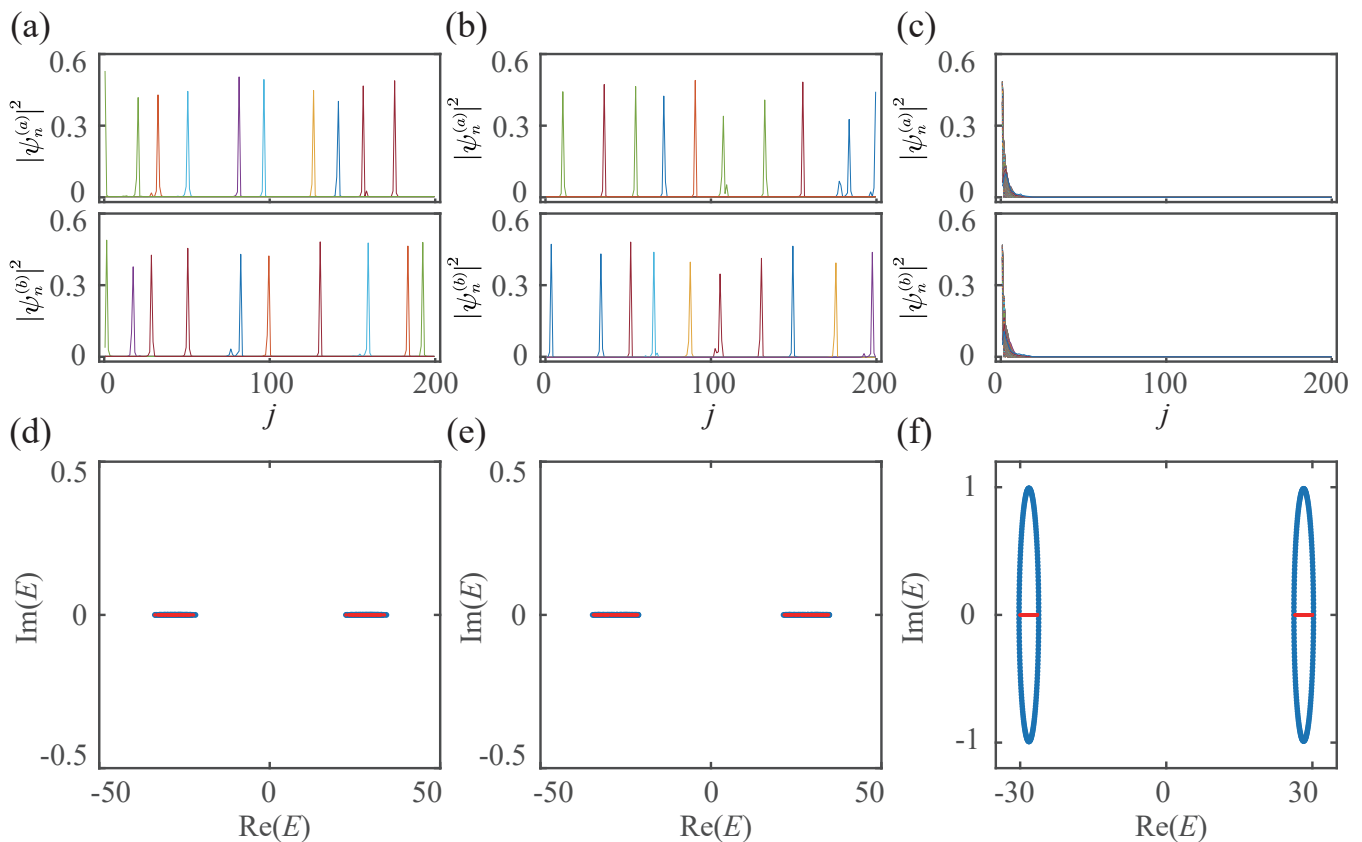


FIG. 2. **Reentrant NHSE under anti-symmetric disorder.** **a-c** Probability density distributions $|\psi_n^{(a)}(j)|^2$ and $|\psi_n^{(b)}(j)|^2$ of the two coupled chains subject to uncorrelated random potential $\Delta_j^{(a)}$ and $\Delta_j^{(b)}$ (a), symmetric random potential with $\Delta_j^{(a)} = \Delta_j^{(b)} = \Delta_j$ (b), and anti-symmetric random potential with $\Delta_j^{(a)} = -\Delta_j^{(b)} = \Delta_j$ (c). Only few eigenstates are plotted in (a) and (b). Plots in (d-f) are the corresponding eigenenergies in the complex plane for PBC (blue dots) and OBC (red dots). The parameters used are $\gamma/J = \lambda/J = 1$, $W/J = 12$, $t/J = 28$, and $N = 200$.

results in reentrant NHSEs, even for arbitrarily strong disorder under the anti-symmetric disorder configuration.

To further study the Anderson localization-delocalization properties caused by the coupling strength t and asymmetric hopping λ , we calculate the inverse participation ratio (IPR) of each normalized eigenstate $\psi_n = (\psi_n^{(a)}, \psi_n^{(b)})^T$, defined as

$$\text{IPR}_n = \sum_j \left(|\psi_n^{(a)}(j)|^4 + |\psi_n^{(b)}(j)|^4 \right), \quad (2)$$

where the sums run over the length N of the coupled chains, $\text{IPR}_n \simeq 1/(2N)$ if the n th eigenstate ψ_n is extended, and drops to zero for an infinite system. In contrast, for eigenstates localized on M sites ($M \ll N$), $\text{IPR}_n \simeq 1/M$, and remains finite for an infinite system. IPR cannot distinguish the skin-boundary modes from the Anderson-localized modes. The skin modes can be resolved by calculating the average eigenstate localization in the form of the mean center of mass (mcom) of the amplitude squared of all eigenvectors ψ_n , averaged over

the disorder realization [61], i.e.,

$$\text{mcom} = \frac{\sum_{j=1}^N j \langle \mathcal{A}(j) \rangle}{\sum_{j=1}^N \langle \mathcal{A}(j) \rangle}, \quad (3)$$

with

$$\langle \mathcal{A}(j) \rangle = \left\langle \frac{1}{2N} \sum_{n=1}^{2N} \left(|\psi_n^{(a)}(j)|^2 + |\psi_n^{(b)}(j)|^2 \right) \right\rangle. \quad (4)$$

where $\langle \cdot \rangle$ indicates disorder averaging. When mcom is close to be 1 or L , it indicates that most of the eigenstates are localized at the boundaries, with the emergence of NHSE.

Figure 3a plots the IPR averaged over all the eigenmodes and mcom as a function of the inter-chain coupling strength t for $W/J = 12$ and $\lambda/J = 1$. This strong disorder causes Anderson localization for small t . As t increases, an Anderson delocalization occurs, accompanied by the manifestation of the NHSE, where all the modes are localized at the boundary for large t . Furthermore, by fixing the disorder ($W/J = 12$)

and hopping ($t/J = 28$) strength, we calculate the averaged IPR and mcom versus the asymmetric hopping parameter λ , as shown in 3b. First, in the Hermitian case with $\lambda = 0$, the anti-symmetric disorder induces the coexistence of localized and extended states [see IPR_n in Fig. 3c] in the finite-size Hermitian ladder (Note that anti-symmetric disorder causes all the modes to become localized in the thermodynamic limit for the Hermitian case, as explained in the Methods Section). Second, in the non-Hermitian regime, as λ increases beyond a certain value, a delocalization occurs, and all the states become skin modes for anti-symmetric disorder [see Fig. 3b]. In addition, the reentrant skin modes caused by the anti-symmetric disorder can be further manifested by studying the quenched evolution dynamics (see details in Section S1 of Supplementary Materials).

Phase diagram

In order to determine the phase diagrams of the localization to delocalization transitions with the emergence of skin modes, due to the triple interplay of anti-symmetric disorder, nonreciprocal hopping and coupling strength of two chains, we calculate the winding number for different parameters. The winding number in real space is defined as [44]

$$w(E_b) = \frac{1}{N'} \text{Tr}' \left(\hat{Q}^\dagger [\hat{Q}, \hat{X}] \right), \quad (5)$$

where \hat{Q} is a positive-definite Hermitian matrix, which is obtained by the polar decomposition $(\hat{\mathcal{H}} - E_b) = \hat{Q}\hat{P}$, with unitary matrix \hat{P} . \hat{Q} and \hat{P} are related to the singular value decomposition $(\hat{\mathcal{H}} - E_b) = \hat{M}\hat{S}\hat{N}^\dagger$, with $\hat{Q} = \hat{M}\hat{N}^\dagger$ and $\hat{P} = \hat{N}\hat{S}\hat{N}^\dagger$. \hat{X} is the coordinate operator, with $X_{jj',ss'} = j\delta_{j,j'}\delta_{s,s'}$ ($s = a, b$), and Tr' denotes the trace over the middle interval with length N' , where the whole chain is cut off from both ends. This definition of the winding number avoids the effects from the system's boundary.

The phase diagrams, in the presence of anti-symmetric disorder, are shown in Fig. 3d-f, where the phase boundary is clearly observed. We can infer that,

regardless of how large the disorder strength W is, the non-Hermitian skin modes reappear once the coupling strength t between the HN and Hermitian chains becomes large enough [see Fig. 3d]. Moreover, the phase boundary is strongly dependent on the asymmetric hopping strength λ [see Fig. 3e,f]. The phase boundary determined by the real-space winding numbers in this correlated-disorder ladder are the same as the one calculated using mcom in Fig. 3g-i.

Experimental implementation

We now implement electrical circuits to realize the reentrant NHSE of the coupled HN-Hermitian chains induced by the correlated disorder. Figure 4a shows the designed electrical circuit network, where the unit cell, containing two sublattices a_j and b_j , are outlined by the red solid line. For the non-Hermitian chain $\{a_j\}$, the nonreciprocal hopping, denoted by the capacitors $C_\gamma \pm C_\lambda$ in Fig. 4a, between nodes j and $j+1$ is realized by the voltage follower [31]. The circuit diagram of the voltage follower module is shown in Fig. 4b, where the resistor $R = 1 \text{ k}\Omega$ in the voltage follower is used to ensure its stability. For the Hermitian chain $\{b_j\}$, the hopping between nodes j and $j+1$ is realized by the capacitor C_J . The inter-chain coupling is represented by the capacitor C_t . The correlated disorder is simulated by the disordered capacitances $C_j^{(a)}$ and $C_j^{(b)}$. In addition, the inductor L is used to adjust the resonance frequency of the circuit. The fabricated circuit boards are shown in Fig. 4c,d.

The model in Eq. (1) is represented by the circuit Laplacian $J(\omega)$ of the circuit. The Laplacian is defined as the response of the voltage vector \mathbf{V} to the input current vector \mathbf{I} by $\mathbf{I}(\omega) = J(\omega)\mathbf{V}(\omega)$. As shown in Fig. 4a, the circuit Laplacian $J(\omega)$ reads (see details in Section S2 of Supplementary Materials)

$$J(\omega) = i\omega\mathcal{H}_c - \left(2i\omega C_J + i\omega C_t + i\omega C_g + \frac{1}{i\omega L} \right) \mathbb{1}, \quad (6)$$

where $\mathbb{1}$ is the $2N \times 2N$ identity matrix, and \mathcal{H}_c is

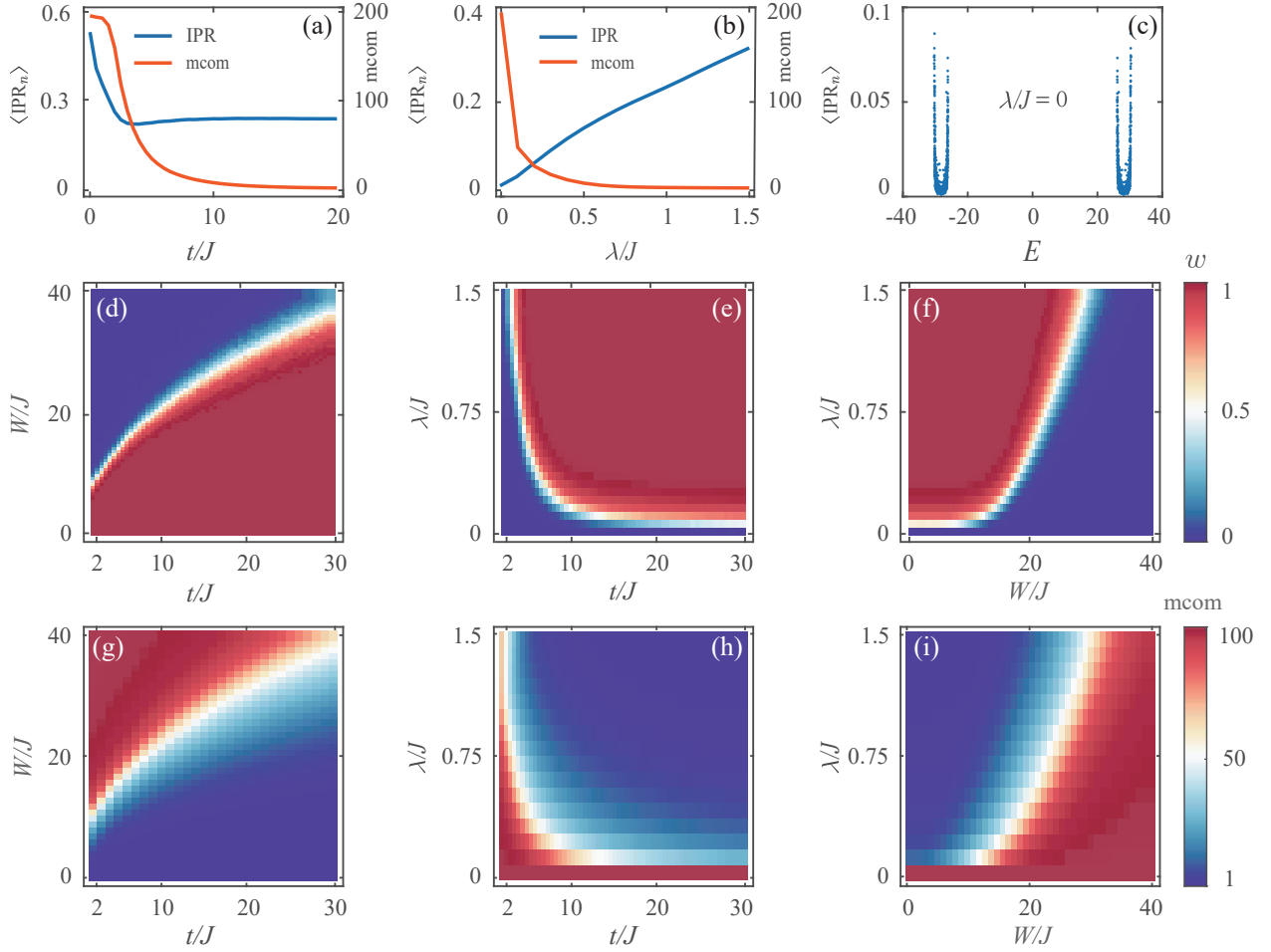
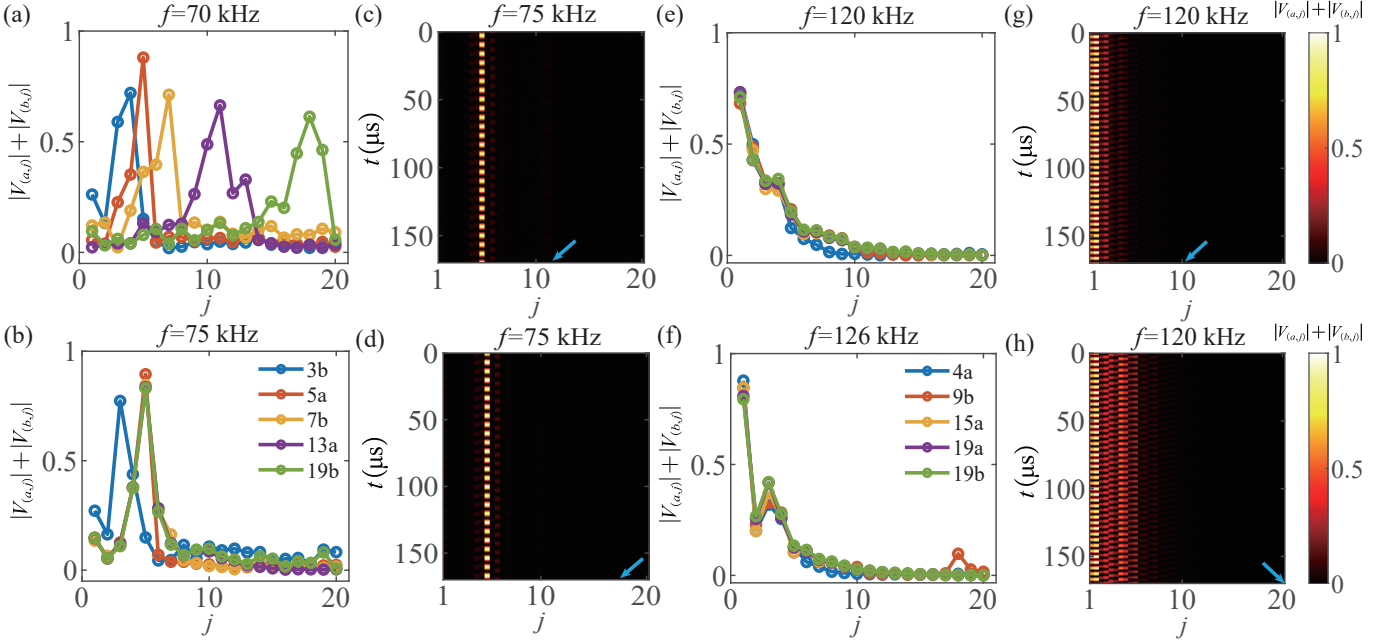
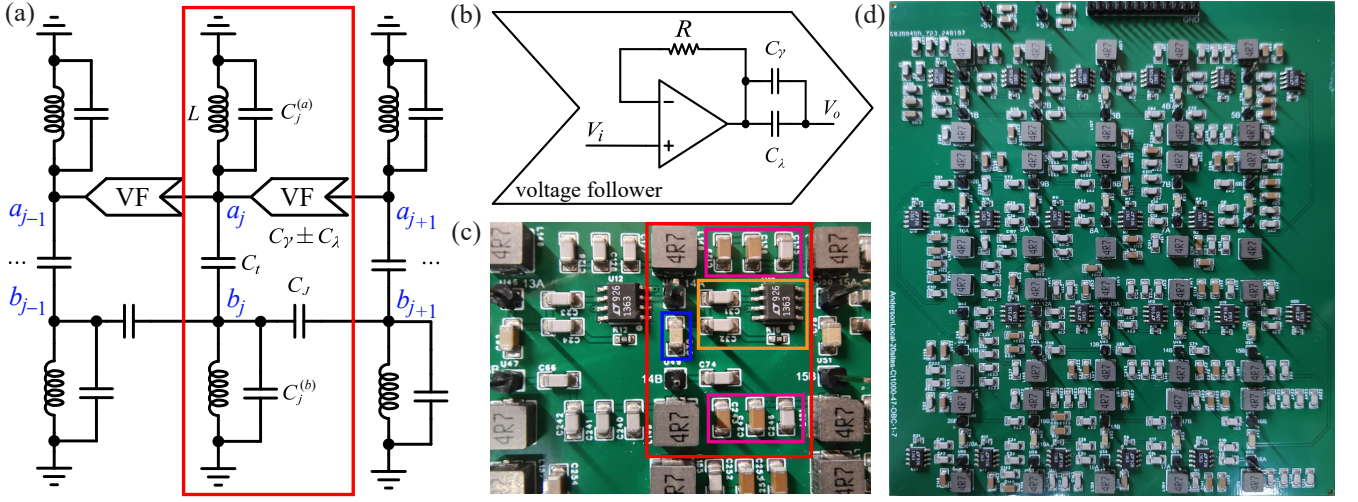


FIG. 3. **IPR, mcom and phase diagram for the occurrence of NHSE subject to anti-symmetric disorder.** **a,b** IPR averaged over all the eigenstates and mcom as a function of the inter-chain coupling strength t for $W/J = 12$ and $\lambda/J = 1$ (**a**), and as a function of the asymmetric hopping strength λ for $W/J = 12$ and $t/J = 28$ (**b**). **c** IPR_n versus E in the coupled two-Hermitian chains under the anti-symmetric disorder. The results are averaged over 2000 disorder realizations with $\gamma/J = 1$ and $N = 400$. **d-f** Winding number w and **g-i** mcom in the (W, t) plane with $\lambda/J = 1$ (**d,g**), the (λ, t) plane with $W/J = 12$ (**e,h**), and the (λ, W) plane with $t/J = 14$ (**f,i**). The results are averaged over 1200 disorder realizations with $\gamma/J = 1$ and $N = 200$.

$$\mathcal{H}_c = \begin{pmatrix} -C_1^{(a)} & C_t & C_J + C_\lambda & 0 & \cdots & 0 & 0 \\ C_t & -C_1^{(b)} & 0 & C_J & \cdots & 0 & 0 \\ C_J - C_\lambda & 0 & -C_2^{(a)} & C_t & \cdots & 0 & 0 \\ 0 & C_J & C_t & -C_2^{(b)} & \cdots & 0 & 0 \\ \vdots & \vdots & \vdots & \vdots & \ddots & \vdots & \vdots \\ 0 & 0 & 0 & 0 & \cdots & -C_L^{(a)} & C_t \\ 0 & 0 & 0 & 0 & \cdots & C_t & -C_L^{(b)} \end{pmatrix}, \quad (7)$$



where $C_J = C_\gamma$ is assumed. According to Eqs. (6) and (7), the circuit Laplacian $J(\omega)$ and \mathcal{H} in Eq. (1) share the same eigenstates if we set $C_J = J$, $C_t = t$, $C_J + C_\lambda = \gamma + \lambda$, $C_J - C_\lambda = \gamma - \lambda$, and $C_j^{(\alpha)} = -\Delta_j^{(\alpha)}$ ($\alpha = a, b$). The eigenstates of $J(\omega)$, corresponding to the circuit frequency $\omega = 2\pi f$, can be obtained by measuring the voltage response at the circuit nodes.

In Fig. 5a,b, we show the measured results of the site-resolved voltage distributions $|V_{a,j}| + |V_{b,j}|$, subject to anti-symmetric disorder at the j th unit cell. We resonantly excite the circuit at different nodes with resonance frequencies $f = 70$ kHz and $f = 75$ kHz, respectively, and then measure the voltages at all the nodes. For weak inter-chain hopping strength C_t , we observe the localized voltages distributions (see Fig. 5a,b). The localized voltage is further verified by measuring the temporal voltage response excited at the 11th and 17th unit cells at the frequency $f = 75$ kHz, as shown in Fig. 5c,d. The voltage remains localized as time evolves, corresponding to the steady voltage distribution in Fig. 5a,b.

We increase the capacitance C_t , i.e. enlarging the inter-chain coupling strength. We resonantly excite the circuit with frequencies $f = 120$ kHz and $f = 126$ kHz, respectively, and then measure the site-resolved voltage distributions $|V_{a,j}| + |V_{b,j}|$ in the presence of the anti-symmetric disorder, as shown in Fig. 5e,f. As predicted theoretically above, we observe the reentrant skin effects of voltage distributions excited at different nodes. Note that the voltage remains localized for the same circuit subject to symmetrically-correlated disorder (see details in Section S3 of the Supplementary Materials). Furthermore, we measure the temporal voltage response excited at the 11th and 20th unit cells at frequency $f = 120$ kHz, as shown in Fig. 5g,h. Once it is excited, the voltage evolves along the sites at the left boundary, indicating the NHSE. Therefore, we have experimentally demonstrated the reentrant NHSE of a disordered nonreciprocal chain, coupled to a Hermitian chain subject to the anti-symmetrical disorder.

Discussion

To conclude, in this combined theoretical and experimental study, we have demonstrated Anderson delocalization and robust NHSE in ultra-strongly disordered coupled HN-Hermitian chains without a Hermitian counterpart. Specifically, although the two coupled Hermitian chains remain always localized in the presence of disorder, the Anderson localization-delocalization can take place when disorder in the HN chain is anti-symmetrically correlated to the one in the Hermitian chain. Moreover, a sufficiently strong inter-chain coupling can always cause Anderson delocalization, accompanied by a reentrant

NHSE, due to the interplay of nonreciprocal hopping and correlated disorder, no matter how strong the disorder is. Furthermore, the Anderson localization-delocalization transition is well captured by the real-space winding number. We finally experimentally verify our theoretical predictions in electrical circuits, where the nonreciprocal hopping is realized by using the voltage follower. The Anderson localization-delocalization transition, accompanied by the NHSE, is observed by measuring the voltage response.

Looking forward, it is interesting to study the reentrant NHSE in disordered higher-dimensional non-Hermitian systems, where its symmetry can also play an important role in determining the Anderson localization-delocalization transition. Moreover, in the future, it is nontrivial to include the effects of interactions on the Anderson localization-delocalization transition and NHSE.

Methods

Physical mechanism. To intuitively understand the physical mechanism of the reentrant NHSE for the strong inter-chain coupling under the anti-symmetric disorder, we consider the concrete case with $|t| \gg |J|, |\gamma \pm \lambda|, |\Delta_j|$ for both symmetric and anti-symmetric disorder. In this case, the inter-chain hopping is the dominant process, and we treat intra-chain hopping terms as perturbation. The Hamiltonian $\hat{\mathcal{H}}$ is thus decomposed as $\hat{\mathcal{H}}_\pm = \hat{\mathcal{H}}_{0,\pm} + \hat{\mathcal{V}}$, with the unperturbed part reading

$$\hat{\mathcal{H}}_{0,\pm} = \sum_j \left[t \left(a_j^\dagger \hat{b}_j + \text{H.c.} \right) + \Delta_j \left(a_j^\dagger a_j \pm \hat{b}_j^\dagger \hat{b}_j \right) \right], \quad (8)$$

and the perturbed part as

$$\begin{aligned} \hat{\mathcal{V}} = & \sum_j \left[(\gamma + \lambda) \hat{a}_j^\dagger \hat{a}_{j+1} + (\gamma - \lambda) \hat{a}_{j+1}^\dagger \hat{a}_j \right] \\ & + \sum_j J \left(\hat{b}_{j+1}^\dagger \hat{b}_j + \text{H.c.} \right), \end{aligned} \quad (9)$$

where $\hat{\mathcal{H}}_+$ denotes the coupled chains under the symmetric disorder effect, and $\hat{\mathcal{H}}_-$ under the anti-symmetric disorder effect.

In the strong inter-chain coupling limit, with $|t| \gg |J|, |\gamma \pm \lambda|, |\Delta_j|$, $\mathcal{H}_{0,\pm}$ can be rewritten as

$$\hat{\mathcal{H}}_{0,\pm} = \sum_{j,m=\pm} \xi_{\pm,j}^{(m)} \hat{\alpha}_{m,j}^\dagger \hat{\alpha}_{m,j}, \quad (10)$$

where $\hat{\alpha}_{\pm,j} = (\pm \hat{a}_j + \hat{b}_j)/\sqrt{2}$, $\xi_{+,j}^\pm = \Delta_j \pm t$, and $\xi_{-,j}^\pm = \pm \sqrt{t^2 + \Delta_j^2}$. In the new basis $|\alpha_{\pm,j}\rangle = \hat{\alpha}_{\pm,j}^\dagger |0\rangle$, we write $\hat{\mathcal{H}}_\pm$ as $\hat{\mathcal{H}}_\pm = \hat{\mathcal{H}}_{0,\pm} + \hat{\mathcal{H}}_{\text{ladder}}$, with

$$\hat{\mathcal{H}}_{\text{ladder}} = \frac{J + \gamma + \lambda}{2} \sum_j \left(\hat{\alpha}_{+,j}^\dagger \hat{\alpha}_{+,j+1} + \alpha_{-,j}^\dagger \hat{\alpha}_{-,j+1} \right) + \frac{J + \gamma - \lambda}{2} \sum_j \left(\hat{\alpha}_{+,j+1}^\dagger \alpha_{+,j} + \hat{\alpha}_{-,j+1}^\dagger \hat{\alpha}_{-,j} \right) \\ + \frac{J - \gamma - \lambda}{2} \sum_j \left(\hat{\alpha}_{-,j}^\dagger \hat{\alpha}_{+,j+1} + \hat{\alpha}_{+,j}^\dagger \hat{\alpha}_{-,j+1} \right) + \frac{J - \gamma + \lambda}{2} \sum_j \left(\alpha_{+,j+1}^\dagger \hat{\alpha}_{-,j} + \hat{\alpha}_{-,j+1}^\dagger \hat{\alpha}_{+,j} \right). \quad (11)$$

In Eq. (11), we have neglected disorder in the hopping terms, which is small for $|\Delta_j| \gg |J|, |\gamma \pm \lambda|$.

In the new basis, $\hat{\mathcal{H}}_{\pm}$ describes a nonreciprocal Creutz ladder $\hat{\mathcal{H}}_{\text{ladder}}$ [60] in the presence of disordered onsite potential $\hat{\mathcal{H}}_{0,\pm}$ for symmetric and anti-symmetric disorder schemes, respectively. For the considered parameters in Fig. 2, $\hat{\mathcal{H}}_{\text{ladder}}$ exhibits a NHSE with all its eigenmodes localized at the left boundary. Under the symmetric disorder scheme, the onsite random potential of the Creutz ladder is given by $\Delta_j \pm t$ for each chain, which leads to Anderson localization for strong disorder Δ_j .

However, for the anti-symmetric disorder case, the onsite random potential of the ladder reads $\pm \sqrt{t^2 + \Delta_j^2}$ for each chain. Then, the disorder strength \tilde{W} of the Creutz ladder becomes $\tilde{W} < W^2/|8t|$. In the strong coupling limit, with $|t| \gg |\Delta_j|$, i.e., $|t| \gg W$, the disorder strength \tilde{W} of the Creutz ladder is much smaller than the asymmetric hopping strength λ . Although an arbitrarily small amount of disorder leads to Anderson localization in 1D Hermitian systems [51], it has been shown that the interplay of nonreciprocal hopping and disorder causes Anderson transition [36, 39]. Therefore, the increasing inter-chain hopping t eventually results in reentrant NHSEs, even for arbitrarily strong disorder under the anti-symmetric disorder configuration.

Circuit construction and measurements. A printed circuit board (PCB) layout is simulated using LTSpice, designed and manufactured using LCEA. The non-reciprocal hopping is implemented using voltage followers based on the unity-gain stable operational amplifier model LT1363. In the circuit, 1 k Ω ($\pm 1\%$ tolerance) resistors are employed to maintain the stability of the operational amplifier, and 100 nF ($\pm 10\%$ tolerance) and 2.2 μF ($\pm 10\%$ tolerance) capacitors are used to suppress ripple noise from the direct current (DC) power supply.

To measure eigenstates, a signal generator (Keysight 33500B) is used to generate a chirp signal, which is then injected into the circuit. The voltage response to this signal is recorded using an oscilloscope (Keysight DSOX4024A) to diagnose the resonance frequency f . With this frequency f , the circuit is excited at a certain node, and the voltage response is measured on all nodes to obtain the eigenstates. For temporal measurements,

the signal generator is utilized to produce a sinusoidal signal with frequency f and duration of 150 μs , and this signal is injected to a certain node of the circuit. The oscilloscope then measures the voltage response at all the nodes to obtain the time-evolving states.

Data availability

The data presented in the figures and that support the other findings of this study are available from the corresponding author on reasonable request.

Code availability

The codes are available upon reasonable request from the corresponding author.

Acknowledgments

T.L. acknowledges the support from the National Natural Science Foundation of China (Grant No. 12274142), the Fundamental Research Funds for the Central Universities (Grant No. 2023ZYGXZR020), Introduced Innovative Team Project of Guangdong Pearl River Talents Program (Grant No. 2021ZT09Z109), and the Startup Grant of South China University of Technology (Grant No. 20210012). Y.R.Z. thanks the support from the National Natural Science Foundation of China (Grant No. 12475017) and Natural Science Foundation of Guangdong Province (Grant No. 2024A1515010398). W.J. thanks the support from the National Natural Science Foundation of China (No. U21A2093) and Introduced Innovative Team Project of Guangdong Pearl River Talents Program (Grant No. 2021ZT09Z109). F.N. is supported in part by: Nippon Telegraph and Telephone Corporation (NTT) Research, the Japan Science and Technology Agency (JST) [via the CREST Quantum Frontiers program Grant No. JPMJCR24I2, the Quantum Leap Flagship Program (Q-LEAP), and the Moonshot R&D Grant Number JPMJMS2061], and the Office of Naval Research (ONR) Global (via Grant No. N62909-23-1-2074).

Author contributions

T.L. conceived the original concept and initiated the work. X.W., W.J. and W.W.J. designed the experiment and fabricated the device. T.L., X.W., Y.R.Z., X.Q.H. and J.L. performed numerical simulations and theoretical explanations. All authors contributed to

the experimental setup, discussions of the results, and the development of the manuscript. Z.Y. and F.N. supervised the whole project.

Competing interests

The authors declare no competing interests.

Additional information

Supplementary information. The online version contains supplementary material.

-
- * These authors contributed equally
 † E-mail: wjuphy@scut.edu.cn
 ‡ E-mail: liutao0716@scut.edu.cn
 § E-mail: yangzm@scut.edu.cn
- [1] D. Leykam, K. Y. Bliokh, C. Huang, Y. D. Chong, and F. Nori, “Edge modes, degeneracies, and topological numbers in non-Hermitian systems,” *Phys. Rev. Lett.* **118**, 040401 (2017).
 - [2] R. El-Ganainy, K. G. Makris, M. Khajavikhan, Z. H. Musslimani, S. Rotter, and D. N. Christodoulides, “Non-Hermitian physics and PT symmetry,” *Nat. Phys.* **14**, 11 (2018).
 - [3] S. Yao and Z. Wang, “Edge states and topological invariants of non-Hermitian systems,” *Phys. Rev. Lett.* **121**, 086803 (2018).
 - [4] K. Yokomizo and S. Murakami, “Non-Bloch band theory of non-Hermitian systems,” *Phys. Rev. Lett.* **123**, 066404 (2019).
 - [5] T. Liu, Y.-R. Zhang, Q. Ai, Z. Gong, K. Kawabata, M. Ueda, and F. Nori, “Second-order topological phases in non-Hermitian systems,” *Phys. Rev. Lett.* **122**, 076801 (2019).
 - [6] K. Zhang, Z. Yang, and C. Fang, “Correspondence between winding numbers and skin modes in non-Hermitian systems,” *Phys. Rev. Lett.* **125**, 126402 (2020).
 - [7] N. Okuma, K. Kawabata, K. Shiozaki, and M. Sato, “Topological origin of non-Hermitian skin effects,” *Phys. Rev. Lett.* **124**, 086801 (2020).
 - [8] K. Kawabata, T. Bessho, and M. Sato, “Classification of exceptional points and non-Hermitian topological semimetals,” *Phys. Rev. Lett.* **123**, 066405 (2019).
 - [9] Z. Y. Ge, Y. R. Zhang, T. Liu, S. W. Li, H. Fan, and F. Nori, “Topological band theory for non-Hermitian systems from the Dirac equation,” *Phys. Rev. B* **100**, 054105 (2019).
 - [10] H. Zhao, X. Qiao, T. Wu, B. Midya, S. Longhi, and L. Feng, “Non-Hermitian topological light steering,” *Science* **365**, 1163 (2019).
 - [11] K. Kawabata, K. Shiozaki, M. Ueda, and M. Sato, “Symmetry and topology in non-Hermitian physics,” *Phys. Rev. X* **9**, 0411015 (2019).
 - [12] D. S. Borgnia, A. J. Kruchkov, and R.-J. Slager, “Non-Hermitian boundary modes and topology,” *Phys. Rev. Lett.* **124**, 056802 (2020).
 - [13] T. Liu, J. J. He, T. Yoshida, Z.-L. Xiang, and F. Nori, “Non-Hermitian topological Mott insulators in one-dimensional fermionic superlattices,” *Phys. Rev. B* **102**, 235151 (2020).
 - [14] T. Liu, J. J. He, Z. Yang, and F. Nori, “Higher-order Weyl-exceptional-ring semimetals,” *Phys. Rev. Lett.* **127**, 196801 (2021).
 - [15] S. Mu, L. Zhou, L. Li, and J. Gong, “Non-Hermitian pseudo mobility edge in a coupled chain system,” *Phys. Rev. B* **105**, 205402 (2022).
 - [16] K. Li and Y. Xu, “Non-Hermitian absorption spectroscopy,” *Phys. Rev. Lett.* **129**, 093001 (2022).
 - [17] Z. Ren, D. Liu, E. Zhao, C. He, K. K. Pak, J. Li, and G.-B. Jo, “Chiral control of quantum states in non-Hermitian spin-orbit-coupled fermions,” *Nat. Phys.* **18**, 385 (2022).
 - [18] K. Kawabata, T. Numasawa, and S. Ryu, “Entanglement phase transition induced by the non-Hermitian skin effect,” *Phys. Rev. X* **13**, 021007 (2023).
 - [19] Z.-F. Cai, T. Liu, and Z. Yang, “Non-Hermitian skin effect in periodically driven dissipative ultracold atoms,” *Phys. Rev. A* **109**, 063329 (2024).
 - [20] A. Regensburger, C. Bersch, M. A. Miri, G. Onishchukov, D. N. Christodoulides, and U. Peschel, “Parity-time synthetic photonic lattices,” *Nature* **488**, 167 (2012).
 - [21] H. Jing, S. K. Özdemir, X. Y. Lü, J. Zhang, L. Yang, and F. Nori, “ \mathcal{PT} -symmetric phonon laser,” *Phys. Rev. Lett.* **113**, 053604 (2014).
 - [22] H. Hodaei, M. A. Miri, M. Heinrich, D. N. Christodoulides, and M. Khajavikhan, “Parity-time-symmetric microring lasers,” *Science* **346**, 975 (2014).
 - [23] B. Peng, Ş. K. Özdemir, F. Lei, F. Monifi, M. Gianfreda, G. L. Long, S. Fan, F. Nori, C. M. Bender, and L. Yang, “Parity-time-symmetric whispering-gallery microcavities,” *Nat. Phys.* **10**, 394 (2014).
 - [24] B. Peng, Ş. K. Özdemir, S. Rotter, H. Yilmaz, M. Liertzer, F. Monifi, C. M. Bender, F. Nori, and L. Yang, “Loss-induced suppression and revival of lasing,” *Science* **346**, 328 (2014).
 - [25] C. Leefmans, A. Dutt, J. Williams, L. Yuan, M. Parto, F. Nori, S. Fan, and A. Marandi, “Topological dissipation in a time-multiplexed photonic resonator network,” *Nat. Phys.* **18**, 442 (2022).
 - [26] M. Parto, C. Leefmans, J. Williams, F. Nori, and A. Marandi, “Non-Abelian effects in dissipative photonic topological lattices,” *Nat. Commun.* **14**, 1440 (2023).
 - [27] C. R. Leefmans, M. Parto, J. Williams, A. Dutt G. H. Y. Li, F. Nori, and A. Marandi, “Topological temporally mode-locked laser,” *Nat. Phys.* **20**, pages852 (2024).
 - [28] J. Zhang, B. Peng, Ş. K. Özdemir, K. Pichler, D. O. Krimer, G. Zhao, F. Nori, Y. X. Liu, S. Rotter, and L. Yang, “A phonon laser operating at an exceptional point,” *Nat. Photon.* **12**, 479 (2018).
 - [29] Y. Choi, C. Hahn, J. W. Yoon, and S. H. Song, “Observation of an anti-PT-symmetric exceptional point and energy-difference conserving dynamics in electrical circuit resonators,” *Nat. Commun.* **9**, 2182 (2018).
 - [30] T. Helbig, T. Hofmann, S. Imhof, M. Abdelghany, T. Kiessling, L. W. Molenkamp, C. H. Lee, A. Szameit, M. Greiter, and R. Thomale, “Generalized bulk-boundary correspondence in non-Hermitian topolelectrical circuits,” *Nat. Phys.* **16**, 747 (2020).
 - [31] J. Wu, Z. Wang, Y. Biao, F. Fei, S. Zhang, Z. Yin, Y. Hu, Z. Song, T. Wu, F. Song, and R. Yu, “Non-Abelian gauge fields in circuit systems,” *Nat. Electron.* **5**, 635 (2022).
 - [32] D. Zou, T. Chen, W. He, J. Bao, C. H. Lee, H. Sun, and X. Zhang, “Observation of hybrid higher-order skin-

- topological effect in non-Hermitian topoelectrical circuits,” *Nat. Commun.* **12**, 7201 (2021).
- [33] J. Hu, R.-Y. Zhang, Y. Wang, X. Ouyang, Y. Zhu, H. Jia, and C. T. Chan, “Non-Hermitian swallowtail catastrophe revealing transitions among diverse topological singularities,” *Nat. Phys.* **19**, 1098 (2023).
- [34] K. Yamamoto, M. Nakagawa, K. Adachi, K. Takasan, M. Ueda, and N. Kawakami, “Theory of non-Hermitian fermionic superfluidity with a complex-valued interaction,” *Phys. Rev. Lett.* **123**, 123601 (2019).
- [35] M. Nakagawa, N. Tsuji, N. Kawakami, and M. Ueda, “Dynamical sign reversal of magnetic correlations in dissipative Hubbard models,” *Phys. Rev. Lett.* **124**, 147203 (2020).
- [36] N. Hatano and D. R. Nelson, “Localization transitions in non-Hermitian quantum mechanics,” *Phys. Rev. Lett.* **77**, 570 (1996).
- [37] N. Hatano and D. R. Nelson, “Non-Hermitian delocalization and eigenfunctions,” *Phys. Rev. B* **58**, 8384 (1998).
- [38] J. Feinberg and A. Zee, “Non-Hermitian localization and delocalization,” *Phys. Rev. E* **59**, 6433 (1999).
- [39] Z. Gong, Y. Ashida, K. Kawabata, K. Takasan, S. Higashikawa, and M. Ueda, “Topological phases of non-Hermitian systems,” *Phys. Rev. X* **8**, 031079 (2018).
- [40] H. Jiang, L.-J. Lang, C. Yang, S.-L. Zhu, and S. Chen, “Interplay of non-Hermitian skin effects and Anderson localization in nonreciprocal quasiperiodic lattices,” *Phys. Rev. B* **100**, 054301 (2019).
- [41] C. Wang and X. R. Wang, “Level statistics of extended states in random non-Hermitian Hamiltonians,” *Phys. Rev. B* **101**, 165114 (2020).
- [42] S. Longhi, “Topological phase transition in non-Hermitian quasicrystals,” *Phys. Rev. Lett.* **122**, 237601 (2019).
- [43] A. F. Tzortzakakis, K. G. Makris, and E. N. Economou, “Non-Hermitian disorder in two-dimensional optical lattices,” *Phys. Rev. B* **101**, 014202 (2020).
- [44] J. Claes and Taylor L. Hughes, “Skin effect and winding number in disordered non-Hermitian systems,” *Phys. Rev. B* **103**, L140201 (2021).
- [45] X. Luo, T. Ohtsuki, and R. Shindou, “Universality classes of the Anderson transitions driven by non-Hermitian disorder,” *Phys. Rev. Lett.* **126**, 090402 (2021).
- [46] K. Kawabata and S. Ryu, “Nonunitary scaling theory of non-Hermitian localization,” *Phys. Rev. Lett.* **126**, 166801 (2021).
- [47] C. C. Wanjura, M. Brunelli, and A. Nunnenkamp, “Correspondence between non-Hermitian topology and directional amplification in the presence of disorder,” *Phys. Rev. Lett.* **127**, 213601 (2021).
- [48] S. Weidemann, M. Kremer, S. Longhi, and A. Szameit, “Coexistence of dynamical delocalization and spectral localization through stochastic dissipation,” *Nat. Photon.* **15**, 576 (2021).
- [49] Q. Lin, T. Li, L. Xiao, K. Wang, W. Yi, and P. Xue, “Observation of non-Hermitian topological Anderson insulator in quantum dynamics,” *Nat. Commun.* **13**, 3229 (2022).
- [50] H. Liu, M. Lu, Z.-Q. Zhang, and H. Jiang, “Modified generalized Brillouin zone theory with on-site disorder,” *Phys. Rev. B* **107**, 144204 (2023).
- [51] E. Abrahams, P. W. Anderson, D. C. Licciardello, and T. V. Ramakrishnan, “Scaling theory of localization: Absence of quantum diffusion in two dimensions,” *Phys. Rev. Lett.* **42**, 673 (1979).
- [52] P. W. Brouwer, C. Mudry, B. D. Simons, and A. Altland, “Delocalization in coupled one-dimensional chains,” *Phys. Rev. Lett.* **81**, 862 (1998).
- [53] H. C. F. Martens, “Delocalization in weakly coupled disordered wires: Application to conjugated polymers,” *Phys. Rev. Lett.* **96**, 076603 (2006).
- [54] D. Weinmann and S. N. Evangelou, “Parity-dependent localization in n strongly coupled chains,” *Phys. Rev. B* **90**, 155411 (2014).
- [55] P. Bordia, H. P. Lüschen, S. S. Hodgman, M. Schreiber, I. Bloch, and U. Schneider, “Coupling identical one-dimensional many-body localized systems,” *Phys. Rev. Lett.* **116**, 140401 (2016).
- [56] T. Iadecola and M. Žnidarič, “Exact localized and ballistic eigenstates in disordered chaotic spin ladders and the Fermi-Hubbard model,” *Phys. Rev. Lett.* **123**, 036403 (2019).
- [57] X. Lin and M. Gong, “Fate of localization in a coupled free chain and a disordered chain,” *Phys. Rev. A* **109**, 033310 (2024).
- [58] X. Lin, M. Gong, and G.-C. Guo, “From single-particle to many-body mobility edges and the fate of overlapped spectra in coupled disorder models,” arXiv:2307.01638 (2023).
- [59] S. Liu, R. Shao, S. Ma, L. Zhang, Oubo You, H. Wu, Y. J. Xiang, T. J. Cui, and S. Zhang, “Non-Hermitian skin effect in a non-Hermitian electrical circuit,” *Research* **2021**, 5608038 (2021).
- [60] M. Creutz, “End states, ladder compounds, and domain-wall fermions,” *Phys. Rev. Lett.* **83**, 2636 (1999).
- [61] P. Molognini, O. Arandes, and E. J. Bergholtz, “Anomalous skin effects in disordered systems with a single non-Hermitian impurity,” *Phys. Rev. Res.* **5**, 033058 (2023).

SUPPLEMENTAL MATERIAL FOR “REENTRANT NON-HERMITIAN SKIN EFFECT INDUCED BY CORRELATED DISORDER”

I. S1. Quenched dynamics

The reentrant skin modes caused by anti-symmetric disorder can be further examined by studying the quenched evolution dynamics. The initial state is chosen as a Gaussian wavepacket as $\psi_0(j) = \exp[-(j - j_0)^2/2\sigma^2]/\mathcal{N}$ centered at the site j_0 , where \mathcal{N} is the normalization constant, and σ denotes the wavepacket width. The wavefunction at time τ is obtained by numerically calculating $|\psi(j, \tau)\rangle = \exp(-i\mathcal{H}\tau) |\psi_0(j)\rangle$. Figure S1 plots quenched dynamics of density distributions for different λ subjected to anti-symmetric disorder, where the hopping strength suddenly changes from $t/J = 1$ to $t/J = 28$ at time $\tau = 50$. For the Hermitian case with $\lambda/J = 0$ [see Fig. S1(a1)], the initial localized mode remains mostly localized after the quench. The slight spreading of the density distribution is attributed to finite-size effects. As the asymmetric hopping parameter λ increases, the wavepacket initially localized at the center of the ladder becomes delocalized, and propagates towards the left boundary after the quench, and it is finally localized at the boundary, due to the interplay of the NHSE and anti-symmetric disorder.

II. S2. Circuit Implementation of the model

In this section, we present a detailed circuit implementation of our model. Linear circuit networks, composed of linear components, can be characterized by a series of time-dependent differential equations. After applying the Fourier transformation with respect to time, these equations can be simplified into a set of algebraic equations in the

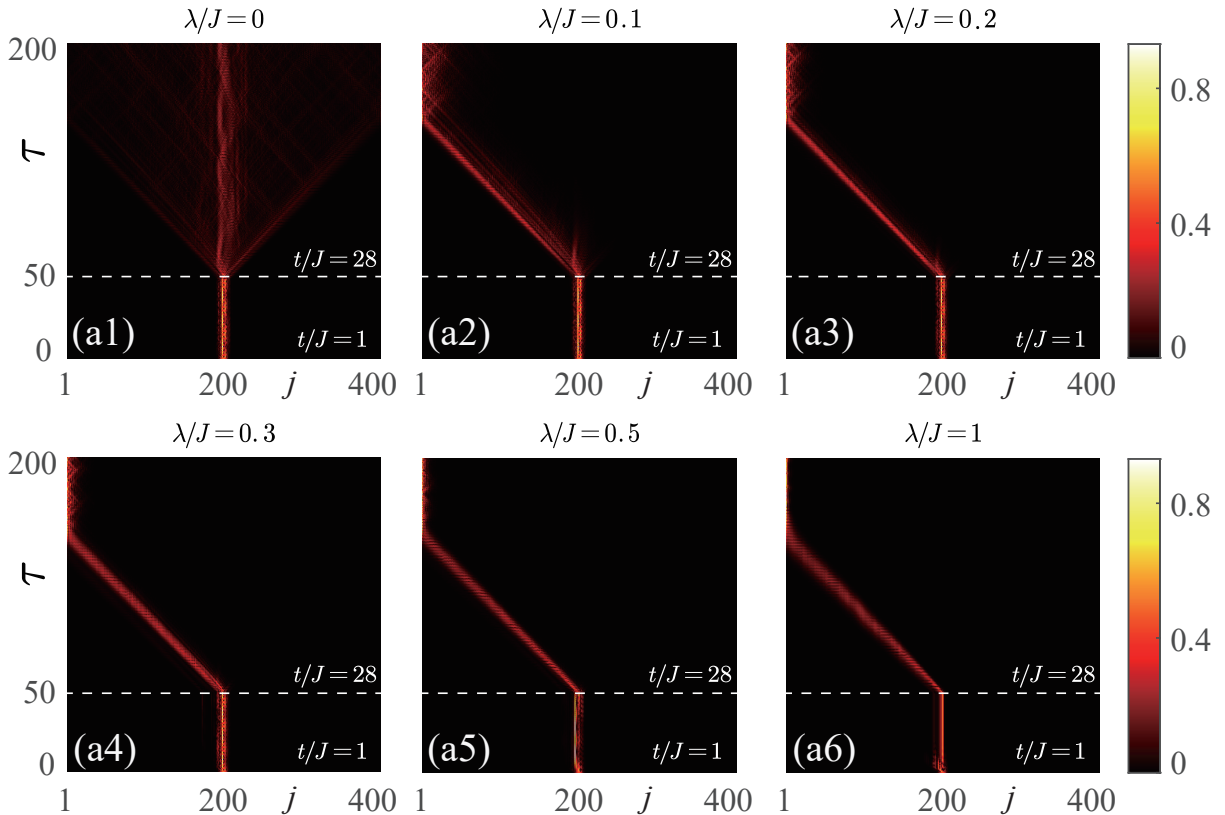


FIG. S1. **Dynamical localization and delocalization via quench.** Quenched dynamics of density distributions for different λ subjected to anti-symmetric disorder, where the initial state is set as the Gaussian wavepacket as $\psi_0(j) = \exp[-(j - j_0)^2/2\sigma^2]/\mathcal{N}$ centered at the site j_0 in the HN chain. At time $\tau = 50$, the hopping strength changes from $t/J = 1$ to $t/J = 28$. The parameters used are $\gamma/J = 1$, $W/J = 12$, and $N = 400$ with (a1) $\lambda/J = 0$, (a2) $\lambda/J = 0.1$, (a3) $\lambda/J = 0.2$, (a4) $\lambda/J = 0.3$, (a5) $\lambda/J = 0.5$, and (a6) $\lambda/J = 1$.

frequency domain. In the frequency domain, the relation of current and voltage between two nodes can be written as

$$I_{jk}(\omega) = \frac{V_j(\omega) - V_k(\omega)}{Z_{jk}(\omega)}, \quad (\text{S1})$$

where $Z_{jk}(\omega)$ is the impedance between node j and node k , and the impedances of capacitor, inductor and resistor are $Z_C(\omega) = 1/i\omega C$, $Z_L(\omega) = i\omega L$ and $Z_R(\omega) = R$. According to Kirchhoff's current law, the sum of all currents entering and leaving a node equals zero. This indicates that the input current I_j at the node j equals the sum of the currents leaving node j :

$$I_j = \sum_k I_{jk}. \quad (\text{S2})$$

According to Eqs. (S1) and (S2), we can derive the circuit Laplacian of the electrical circuit in Fig. S2(a), corresponding to the tight-binding lattice model in Fig. S2(b).

The equivalent circuit of the model is composed of inductors and capacitors. The voltage follower is used to equivalently simulate the non-reciprocal hopping of the model with $\gamma = \lambda$. The circuit diagram of the voltage follower module is shown in Fig. S2(c), where the resistor $R = 1$ k Ω in the voltage follower is used to ensure its stability. Capacitors are used to equivalently simulate the reciprocal hopping and onsite potential of the tight-binding model, where the capacitances of the capacitors C_γ , C_λ , C_t and C_J correspond to the reciprocal hopping strengths γ , λ , t and J in Fig. S2(b). The correlated disorders $\Delta_j^{(a)}$ and $\Delta_j^{(b)}$ are simulated by the disordered capacitances $C_j^{(a)}$ and $C_j^{(b)}$. In addition, the inductor L is used to adjust the resonance frequency of the circuit.

The coupled HN-Hermitian chains in the main text can be represented by the Laplacian $J(\omega)$ of the circuit. The Laplacian is defined as the response of the voltage vector \mathbf{V} to the input current vector \mathbf{I} by

$$\mathbf{I}(\omega) = J(\omega)\mathbf{V}(\omega). \quad (\text{S3})$$

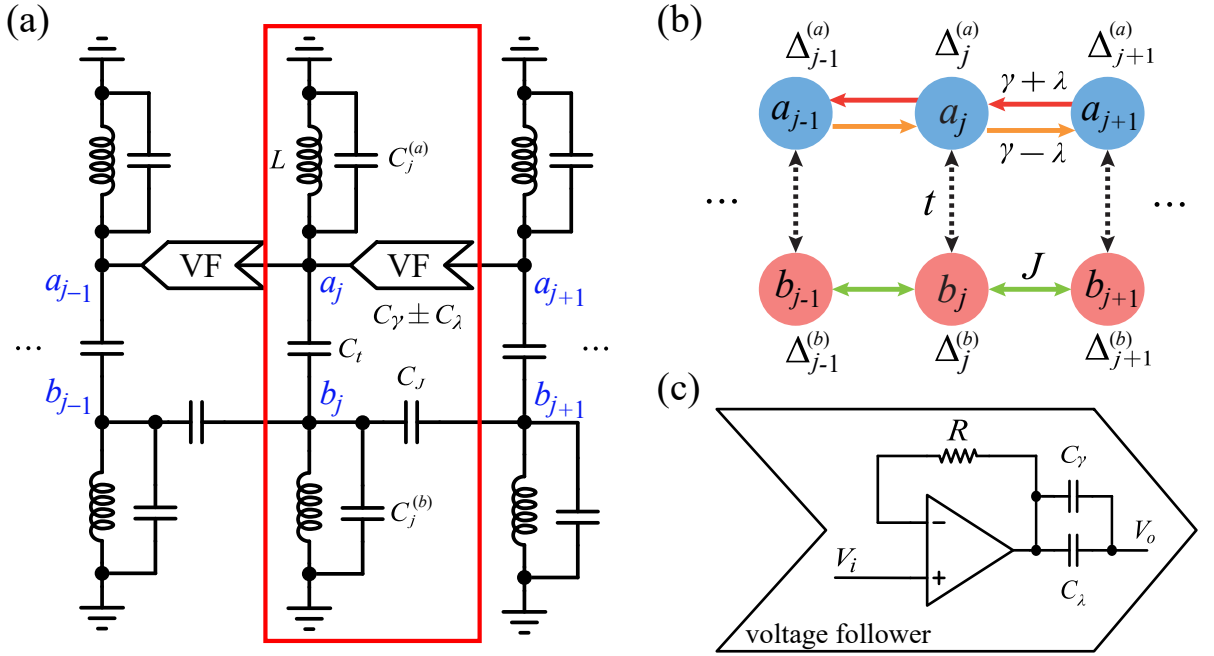


FIG. S2. **Electrical-circuit lattice.** **a** Circuit implementation of the coupled HN-Hermitian lattice subject to correlated disorder, corresponding to the tight-binding lattice model in **(b)**. The red solid line outlines a unit cell, containing two sublattices a_j and b_j , in the circuit lattice. For the HN chain $\{a_j\}$, the nonreciprocal intra-chain hopping, represented by capacitors $C_\gamma \pm C_\lambda$, is realized by the voltage follower (VF). The circuit diagram of the voltage follower module is shown in **(c)**, where the resistor $R = 1$ k Ω in the voltage follower is used to ensure its stability. The capacitor C_J denotes the intra-chain hopping in the Hermitian chain $\{b_j\}$, C_t represents the inter-chain hopping. $C_j^{(a)}$ and $C_j^{(b)}$ are disordered capacitances for simulating the correlated disorder. The inductor L is used to adjust the resonance frequency of the circuit.

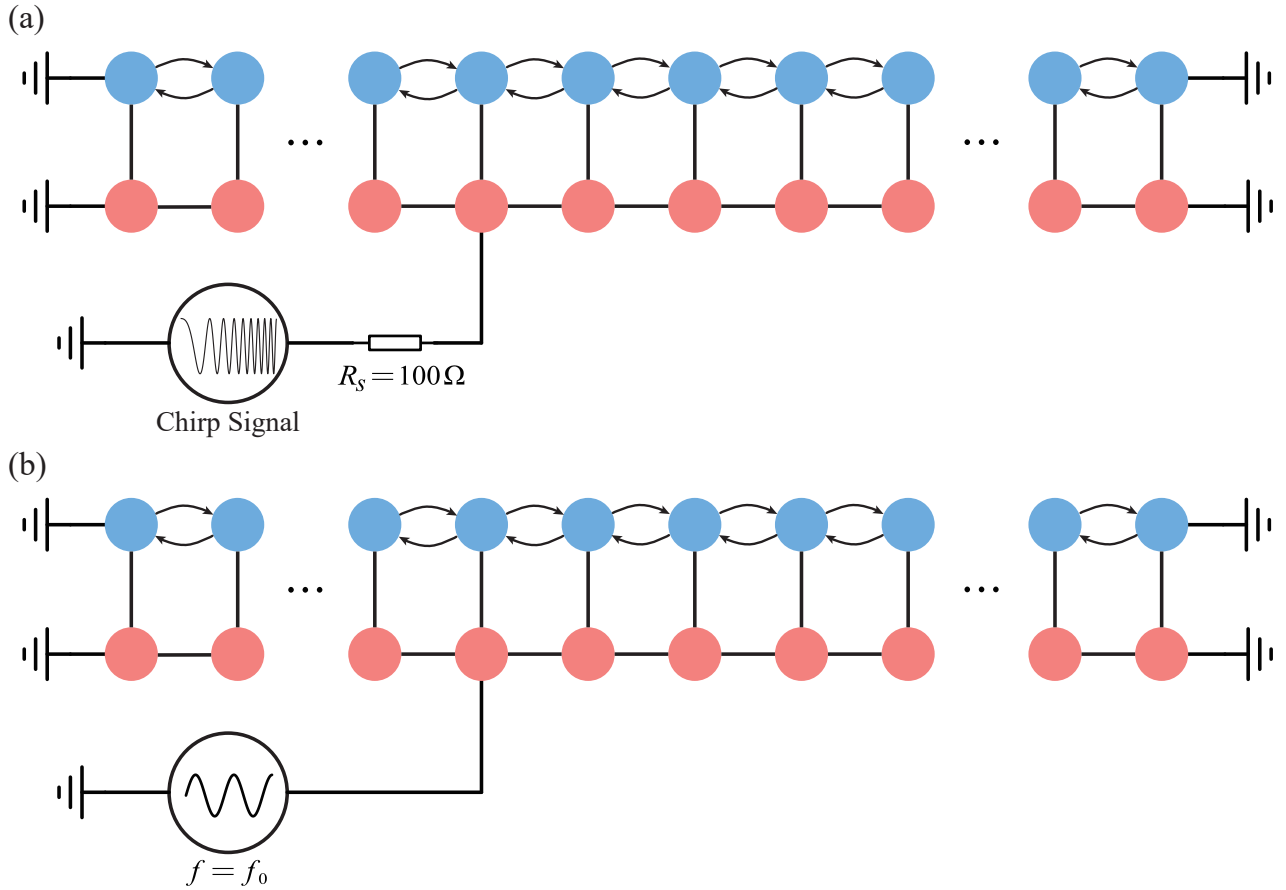


FIG. S3. **Schematic of the experiment.** **a** A chimp signal is used for analyzing the steady-state voltage response at different frequencies. **b** A monochromatic signal is used for measuring the temporal voltage response of the circuit under the specific frequency f_0 .

According to Eq. (S1) and Eq. (S2), the Kirchoff equation of the circuit in Fig. S2(a) is written as

$$I_{a,j} = i\omega(C_\gamma + C_\lambda)(V_{a,j+1} - V_{a,j}) + i\omega(C_\gamma - C_\lambda)(V_{a,j-1} - V_{a,j}) + i\omega C_t(V_{b,j} - V_{a,j}) - i\omega\left(C_g + C_j^{(a)}\right)V_{a,j} - \frac{1}{i\omega L}V_{a,j}, \quad (\text{S4})$$

$$I_{b,j} = i\omega C_t(V_{a,j} - V_{b,j}) + i\omega C_J(V_{b,j+1} - V_{b,j}) + i\omega C_J(V_{b,j-1} - V_{b,j}) - i\omega\left(C_g + C_j^{(b)}\right)V_{b,j} - \frac{1}{i\omega L}V_{b,j}, \quad (\text{S5})$$

where $I_{a,j}$ ($V_{a,j}$) and $I_{b,j}$ ($V_{b,j}$) denote the currents (voltages) on a and b sublattices in the j th cell, respectively, ω denotes the circuit frequency, and C_g is grounded capacitor for ensuring the circuit stability. In experiments, we take $C_\gamma = C_J$. Then, using Eqs. (S4) and (S5), the circuit Laplacian $J(\omega)$ is rewritten as

$$J(\omega) = i\omega\mathcal{H}_c - \left(2i\omega C_J + i\omega C_t + i\omega C_g + \frac{1}{i\omega L}\right)\mathbf{1}, \quad (\text{S6})$$

where $\mathbf{1}$ is the $2N \times 2N$ identity matrix, and \mathcal{H}_c reads

$$\mathcal{H}_c = \begin{pmatrix} -C_1^{(a)} & C_t & C_J + C_\lambda & 0 & \cdots & 0 & 0 \\ C_t & -C_1^{(b)} & 0 & C_J & \cdots & 0 & 0 \\ C_J - C_\lambda & 0 & -C_2^{(a)} & C_t & \cdots & 0 & 0 \\ 0 & C_J & C_t & -C_2^{(b)} & \cdots & 0 & 0 \\ \vdots & \vdots & \vdots & \vdots & \ddots & \vdots & \vdots \\ 0 & 0 & 0 & 0 & \cdots & -C_L^{(a)} & C_t \\ 0 & 0 & 0 & 0 & \cdots & C_t & -C_L^{(b)} \end{pmatrix}, \quad (\text{S7})$$

The matrix \mathcal{H}_c in the first term of the circuit Laplacian $J(\omega)$ in Eq. (S6) replicates the Hamiltonian matrix of the coupled HN-Hermitian chains described in the main text. The second term of the circuit Laplacian $J(\omega)$ in Eq. (S6) does not influence the state localization and delocalization. Therefore, this allows the circuit Laplacian to model the desired Hamiltonian.

When the input current is zero, we can obtain the eigenvalue equation:

$$\mathcal{H}_c \mathbf{V} = \left(2C_J + C_t + C_g - \frac{1}{\omega^2 L} \right) \mathbf{V}. \quad (\text{S8})$$

This indicates that the voltage distribution reflects the state distribution corresponding to the specific eigenvalue by adjusting the frequency $f = \omega/(2\pi)$ of the excited voltage. By measuring the voltage response of the excitation, we can experimentally verify the state delocalization and localization of the coupled HN-Hermitian chains subject to the correlated disorder.

In experiments, we excite the circuit at a certain node, and then test the voltage response at all nodes. The schematic of the testing is shown in Fig. S3. A chirp signal (10 kHz - 400 kHz) is used for analyzing the steady-state voltage response at different frequencies [see Fig. S3(a)]. A monochromatic signal, e.g. sinusoidal wave, is used for measuring the temporal voltage response of the circuit under the specific frequency [see Fig. S3(b)].

III. S3. Experimental results of the NH-Hermitian coupled chains subject to the symmetric disorder

As shown in the main text, the experimental results have proved that the strong inter-chain coupling can lead to the reentrant NHSE in the coupled NH-Hermitian chains in spite of the strong anti-symmetric disorder. In this section, as a comparison, we present experimental results of the coupled NH-Hermitian chains subject to symmetrically-correlated disorder. We resonantly excite the circuit, and measured the site-resolved voltage distributions $|V_{a,j}| + |V_{b,j}|$ in the presence of symmetric disorder. As shown in Fig. S4a,b for weak inter-chain coupling and Fig. S4e,f for strong inter-chain coupling, the voltage distributions remain mostly localized. Furthermore, we measure the temporal voltage response, as shown in Fig. S4c,d for weak inter-chain coupling and Fig. S4g,h for strong inter-chain coupling. Once it is excited, the voltage remains localized as time evolves.

* These authors contributed equally

† E-mail: wjuphy@scut.edu.cn

‡ E-mail: liutao0716@scut.edu.cn

§ E-mail: yangzm@scut.edu.cn

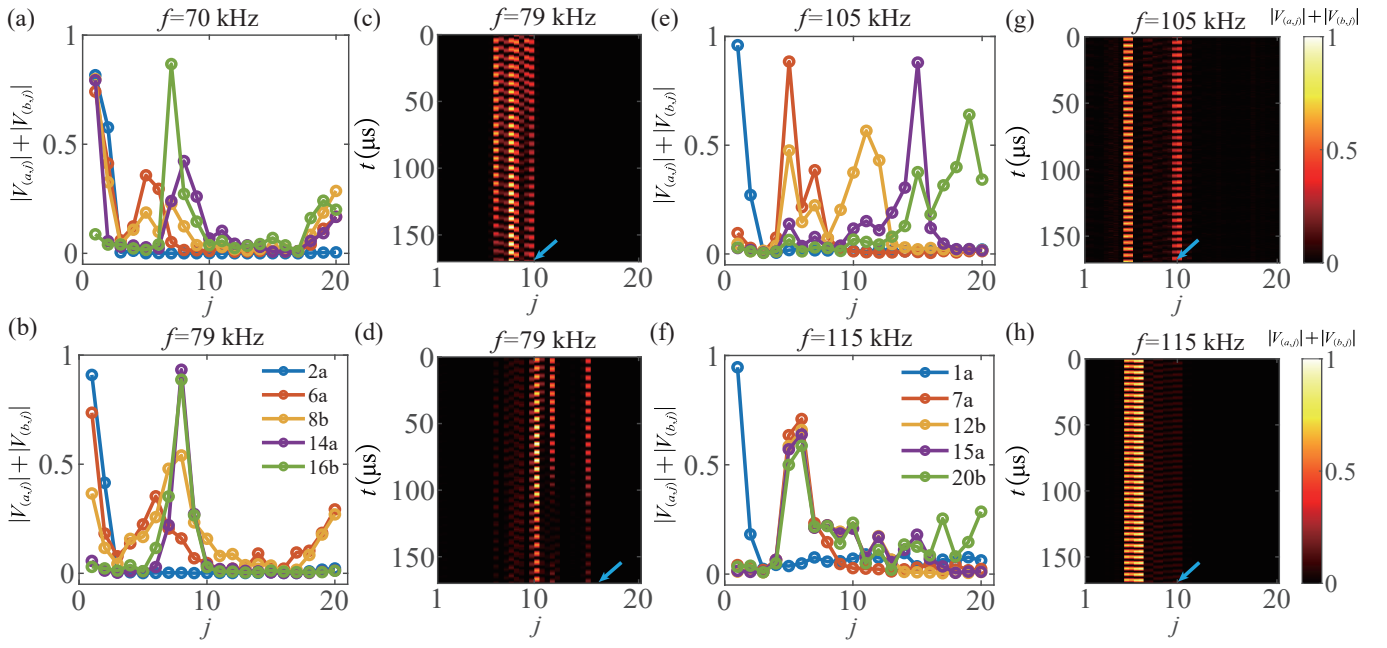


FIG. S4. **Experimental observations of the Anderson localization subject to symmetric disorder.** **a,b** Measured site-resolved voltage distributions $|V_{a,j}| + |V_{b,j}|$ (j is unit-cell index) at resonance frequencies $f = 70$ kHz (**a**) and $f = 79$ kHz (**b**) for weak inter-chain hopping C_t , with $C_\gamma = C_\lambda = C_J = C_t = 100$ nF, $L = 4.7$ μ H, and $C_j^{(a)} = C_j^{(b)} \in [-6C_J, 6C_J]$. The legend “ $j\alpha$ ” ($\alpha = a, b$) in (**b**) indicates the excitation at the j th site of the chain α . **c,d** Measured temporal voltage responses excited at the 11th (**c**) and 17th (**d**) unit cells, indicated by the blue arrows, for the weak inter-chain hopping with $f = 79$ kHz. **e,f** Measured voltage distributions and **g,h** temporal voltage responses for strong inter-chain hopping C_t , with $C_\gamma = C_\lambda = C_J = 47$ nF, $C_t = 1$ μ F, $L = 4.7$ μ H, and $C_j^{(a)} = C_j^{(b)} \in [-6C_J, 6C_J]$.